Accepted Manuscript

Mg/Ca and Sr/Ca as novel geochemical proxies for understanding sediment transport processes within coral reefs

J. Gacutan, A. Vila-Concejo, L.D. Nothdurft, T.E. Fellowes, H.E. Cathey, B.N. Opdyke, D.L. Harris, S. Hamylton, R.C. Carvalho, M. Byrne, J.M. Webster

PII: S0272-7714(17)30091-4

DOI: 10.1016/j.ecss.2017.08.010

Reference: YECSS 5565

To appear in: *Estuarine, Coastal and Shelf Science*

Received Date: 1 February 2017

Revised Date: 26 June 2017

Accepted Date: 8 August 2017

Please cite this article as: Gacutan, J., Vila-Concejo, A., Nothdurft, L.D., Fellowes, T.E., Cathey, H.E., Opdyke, B.N., Harris, D.L., Hamylton, S., Carvalho, R.C., Byrne, M., Webster, J.M., Mg/Ca and Sr/Ca as novel geochemical proxies for understanding sediment transport processes within coral reefs, *Estuarine, Coastal and Shelf Science* (2017), doi: 10.1016/j.ecss.2017.08.010.

Mg/Ca and Sr/Ca as novel geochemical proxies for understanding sediment transport processes within coral reefs

J. Gacutan[a], A. Vila-Concejo[a*], L.D. Nothdurft[b], T. E. Fellowes[a], H. E. Cathey[c], B.N. Opdyke[d], D.L. Harris[a,e] , S. Hamylton[f], R. C. Carvalho[f], M. Byrne[g], J.M. Webster[a]

[a]*Geocoastal Research Group, School of Geosciences, The University of Sydney, Sydney, Australia*

[b]*School of Natural Resource Sciences, Queensland University of Technology, Brisbane, Australia*

[c]*Institute for Future Environments, Queensland University of Technology, Brisbane, Australia*

[d]*Research School of Earth Sciences, The Australian National University, Canberra, Australia*

[e]*Leibniz Center for Tropical Marine Ecology (ZMT) and Center for Marine Environmental Science (MARUM), Bremen University, Bremen, Germany*

[f]*School of Earth and Environmental Sciences, University of Wollongong, Wollongong, Australia*

[g]*Schools of Medical Sciences and Life and Environmental Sciences (SOLES), The University of Sydney, Australia*

[*] Corresponding author at: Geocoastal Research Group, School of Geosciences, The University of Sydney, Madsen Building (F09), Sydney, NSW 2006, Australia. E-mail address: ana.vilaconcejo@sydney.edu.au

Keywords: Large Benthic Foraminifera, Taphonomy, Coral Reef, Carbonate sediments.

Abstract

Sediment transport is a key driver of reef zonation and biodiversity, where an understanding of sediment dynamics gives insights into past reef processes and allows the prediction of geomorphic responses to changing environmental conditions. However, modal conditions within the back-reef seldom promote sediment transport, hence direct observation is inherently difficult. Large benthic foraminifera (LBF) have previously been employed as 'tracers' to infer sediment transport pathways on coral reefs, as their habitat is largely restricted to the algal flat and post-mortem, their calcium carbonate test is susceptible to sediment transport forces into the back-reef. Foraminiferal test abundance and post-depositional test alteration have been used as proxies for sediment transport, although the resolution of these measures becomes limited by low test abundance and the lack of variation within test alteration. Here we propose the novel use of elemental ratios as a proxy for sediment transport. Two species, *Baculogypsina sphaerulata* and *Calcarina capricornia*, were analysed using a taphonomic index within One Tree and Lady Musgrave reefs, Great Barrier Reef (Australia). Inductively coupled plasma-atomic emission spectrometry (ICP-AES) was used to determine Mg/Ca and Sr/Ca and these ratios were compared with taphonomic data. Decreases in test Mg/Ca accompany increases in Sr/Ca in specimens from algal-flat to lagoonal samples in both species, mirroring trends indicated by taphonomic values, therefore indicating a relationship with test alteration. To delineate mechanisms driving changes in elemental ratios, back-scattered electron (BSE) images, elemental mapping and *in situ* quantitative spot analyses by electron microprobe microanalysis (EPMA) using wavelength dispersive X-ray spectrometers (WDS) were performed on un-altered algal flat and heavily abraded tests for both species. EPMA analyses reveal heterogeneity in Mg/Ca between spines and the test wall, implying the loss of appendages results in a decrease in Mg/Ca. BSE imaging and WDS elemental mapping provided evidence for cementation, facilitated by microbial-boring as the primary cause of increasing Sr/Ca. These novel proxies hold advantages over taphonomic measures and further provide a rapid method to infer sediment transport pathways within back-reef environments.

1. Introduction

Definitions of coral reef stability vary in accordance to different timescales. Whilst reefs are considered vulnerable at short-term ecological timescales, the overall evolution and preservation of reefs as calcium carbonate structures highlights their durability over geological timescales (Perry et al., 2008). An approach to bridge this discrepancy is an understanding of geomorphological processes, specifically sediment transport. Coral reefs are composed primarily of unconsolidated sediment and as such, sediment transport is a key driver of reef zonation and the formation of geomorphic features, including islands and back-reef sand aprons (Hopley et al., 2007). Through affecting the substrate for coral recruitment and habitat for benthic calcifiers, sediment transport impacts biodiversity whilst also developing landforms that are preserved over millennia (Perry et al., 2008). An understanding of sediment dynamics gives insights into past reef processes and allows the prediction of future geomorphic responses to changing boundary conditions.

A current paradigm in the morphological evolution of coral reefs is the concept of reef 'maturity', where the extent of back-reef progradation is correlated to the 'stage' of its development and indication of future morphological states (Hopley et al., 2007). The production and deposition of calcareous sediments leads to the progradation of back-reef sand aprons, which are a ubiquitous feature to carbonate platforms in both modern and ancient reefs (Rankey and Garza-Pérez, 2012). Sediments produced *in situ* by benthic calcifiers on the algal flat are entrained through tidal and wave forcing into the back-reef ('lagoonward', Harris et al., 2011, 2015). The resulting lagoonal infill is considered to be one of the major constructional processes once reefs have reached sea level (Marshall and Davies, 1982). A substantial component of back-reef skeletal debris is the tests ('shells') of symbiont-bearing large benthic foraminifera (LBF), generated from populations that inhabit algal flats at high abundance (Fujita et al., 2009, Doo et al., 2012, 2016). The LBF test is extremely robust whilst the host is living, withstanding considerable wave energy (Briguglio and

Hohenegger, 2011) and chemical dissolution (Engel et al., 2015). However, these properties are quickly lost post-mortem, due to loss of attachments used to anchor the test to the substrate, leading to wave-induced transport into the back-reef (Briguglio and Hohenegger, 2011).

Direct field observation of sediment transport within the back-reef environment is inherently difficult. Previous studies have employed streamer traps (Dolan and Charles, 2003) and optical backscatter sensors (Storlazzi et al., 2004, Vila-Concejo et al., 2015) with limited success. Vila-Concejo et al. (2014) have shown minimal sediment transport lagoonward within modal conditions and thus transport of surficial sediments into the back-reef may be largely restricted to high-energy events (Li et al., 1998, Vila□Concejo and Kench, 2017). In addition, Harris et al. (2015) found that the majority of back reef sedimentary infilling occurred during elevated sea levels between 6,000 and 2,000 cal. BP, implying that back-reef sand aprons may be relict features of higher sea levels. Thus, an opportune 'tracer' is the sand-sized tests of LBF, which have a defined source area (algal flat) and are susceptible to sediment transport processes. On atolls and carbonate platforms, hydrodynamic forcing decreases across the reef flat and sand apron due to depth-limited wave-breaking and bottom friction (Kench and Brander, 2006, Vila-Concejo et al., 2013, Harris et al., 2015), creating gradients of decreasing LBF test abundance lagoonwards (Chun et al., 1997).

Granular interactions with the reef flat and sand apron during transport modify LBF tests ('taphonomic alteration'), leading to fracturing, the loss of spines and abraded test wall (Kotler et al., 1992, Ford and Kench, 2012). The resilience of tests to alteration is species-specific, where those more resilient to chemical and physical wear will disperse further and in greater quantities (Maiklem, 1968, Ford and Kench, 2012). Previous studies have incorporated taphonomic alteration as a qualitative proxy to infer sediment transport pathways within both siliciclastic (Alejo et al., 1999) and carbonate settings (Dawson et al., 2014, Pilarczyk et al., 2014, Fellowes et al., 2016). However, there are limitations to the use of LBF as transport proxies, as inter-reef variation in LBF

assemblage and abundance translates to significant differences in their prevalence and taphonomic state within carbonate deposits. A low abundance of tests lowers the resolution and counteracts the determination of sediment pathways (Fellowes et al., 2016).

Foraminiferal tests have long been used in the reconstruction of paleo-ocean chemistry, as the elemental composition of tests reflects their environment of formation (Erez, 2003). There has been a particular focus on the divalent cations (Mg^{2+} and Sr^{2+}), which substitute for Ca^{2+} during biomineralization of calcium carbonate (Zhang and Dawe, 2000). Few studies have explored the minor and trace element content of shallow-water LBF and all have done so to determine their worth in paleo-reconstruction (Raja et al., 2005, 2007). However, Raja et al. (2005) demonstrate significant seasonal, inter and intra-reef variability of elemental ratios within LBF tests, at ranges which leave them unsuitable as a constrained paleo-proxy. Here we propose elemental ratios of Mg/Ca and Sr/Ca within LBF tests as a geochemical proxy for the average magnitude and direction of sediment transport into the back-reef environment. Two related species widespread across the Indo-Pacific, *Baculogypsina sphaerulata* and *Calcarina capricornia*, were analysed for Mg/Ca and Sr/Ca within the sand aprons of One Tree and Lady Musgrave reefs, Great Barrier Reef (GBR). A qualitative analysis of taphonomic abrasion was conducted (comprehensively presented in Fellowes et al., 2016) and compared with elemental ratios (Mg/Ca and Sr/Ca) determined using Inductively Coupled Plasma – Atomic Emission Spectrometer (ICP-AES). To validate the mechanisms that may drive changes in elemental ratios, the spatial distribution of elemental ratios across the test was mapped using an electron microprobe equipped with wavelength-dispersive spectrometers (WDS), whilst back-scattered electron (BSE) images were used to identify mineral textures. It was hypothesised that the Mg/Ca concentrations within the spines would be different to the concentrations within the test walls; hence, loss of spines due to transport would cause changes in the Mg/Ca elemental ratios. Simultaneously, the differences in Sr/Ca would be driven by microbial action, which has been well documented for deep sea cores (Erez, 2003). The objectives of this

study are: (1) qualitatively analyse taphonomic abrasion in surficial samples; (2) delineate trends in Mg/Ca and Sr/Ca across several sand aprons on two reefs; (3) determine the relationship between taphonomy and elemental composition; and, (4) use quantitative analysis by electron microprobe (EPMA) and BSE imaging to identify mechanisms underlying the observed trends. We present a novel geochemical proxy for the magnitude and direction of sediment transport within carbonate systems, supported by evidence from taphonomic test alteration across a back-reef sand apron.

2. Materials and Methods

Figure 1. Study site showing (**a**) Queensland (QLD), Australia and (**b**) the Capricorn Bunker Group, southern Great Barrier Reef off Queensland, Australia. (**c**) One Tree Reef (OTR, 23°30'S 152°06'E), with the northern (NSA), eastern (ESA), and southern sand apron (SSA). (**d**) Lady Musgrave Reef (LMR, 23°54'S; 152°24'E) and its single sand apron.

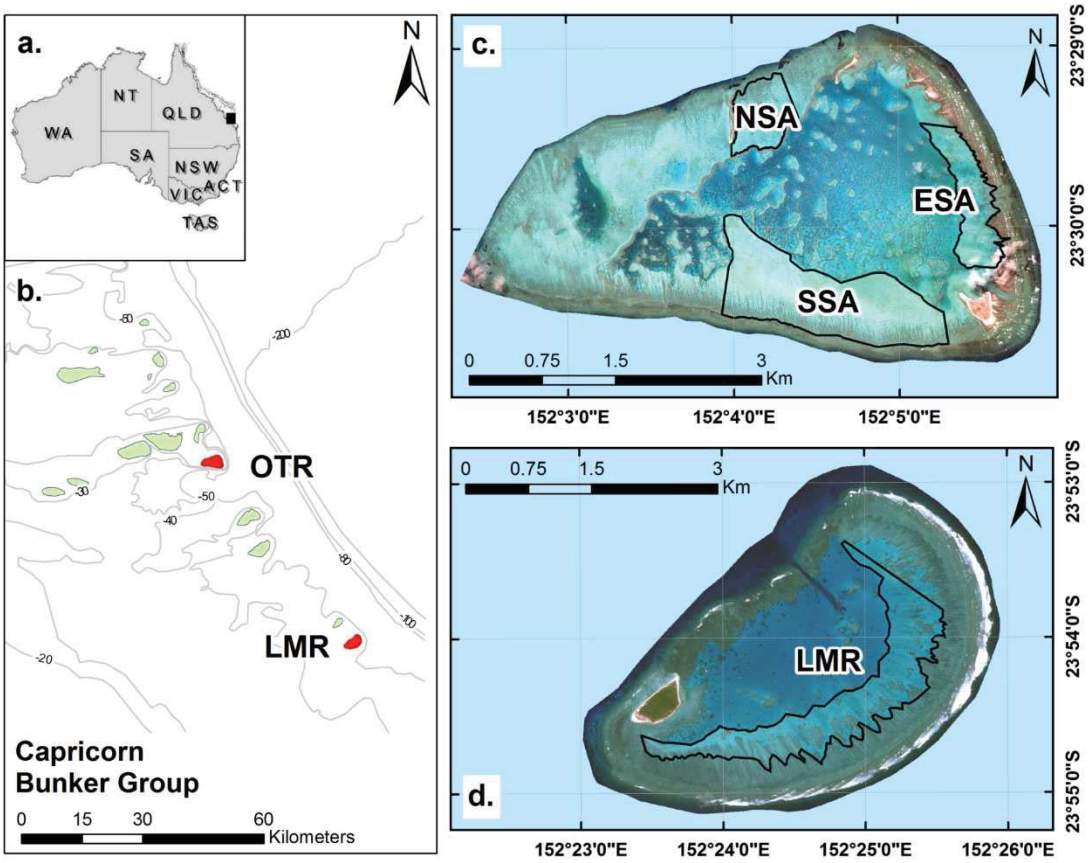

2.1. Study sites

One Tree and Lady Musgrave Reefs are mid-shelf, platform reefs located within the Capricorn Bunker Group in the southern Great Barrier Reef, Australia (Figure 1). The modern reefs overly a karst-modified Pleistocene reef substrate, surrounded by waters approximately 60 m in depth (Orme et al., 1974, Marshall and Davies, 1982). Wind and wave climate is dominated by east-south-easterly swells throughout the year, with modal offshore significant wave heights of 1.15 m (Hopley, 1982). The region is mesotidal and semidiurnal, with a spring tidal range greater than 3 m. Both reefs present clear physiographic zonation, with an algal flat (turfing algae present), reef flat (rubble dominated, no algae), back-reef sand apron, lagoon and scattered patch reefs (Orme et al., 1974, Marshall and Davies, 1982).

One Tree Reef (OTR, Figure 1c) is a lagoonal platform reef (Maxwell, 1968). Under the reef classification by Hopley (1982), the reef is considered 'mature', due to the partial infilling of its lagoons. The height and continuity of the reef flat truncates the tidal cycle, where water level falls below the reef rim at 1.4 m above the lowest astronomical tide, detaching the lagoon from the marine environment for several hours (Ludington, 1979). The southern and eastern margins are exposed to dominant wave energy (windward), whilst the northern margin is protected under modal conditions (leeward). One Tree Reef contains three sand aprons: the southern sand apron (SSA), the eastern sand apron (ESA) and the northern sand apron (NSA). All three sand aprons are backed by algal flats that provide habitat for LBFs, which generate approximately 2800 metric tonnes of sediment yearly (Doo et al., 2012, 2016). The SSA and the NSA also present extensive windrows while the ESA has a well-developed rubble-dominated flat (Figure 1c).

Table 1. Sample collection dates and sand apron descriptions. *_B. sphaerulata_* and _Calcarina_ spp. **_B. sphaerulata_* and _C. capricornia_

Reef	Sand Apron	Total Size (km^2)	Algal flat area (km^2)	Depth (m, below MSL)	Type	Collection Date	Samples analysed for taphonomy*	Samples analysed with ICP-AES**
OTR	SSA	8.22	0.42	0.8 - 1.3	Surficial	May, 2010	25	12
					Living	Apr, 2015	-	3
	ESA	0.53	0.56	0.8 – 2.4	Surficial	Nov, 2014	34	3
					Living	Apr, 2015	-	2
	NSA	0.38	0.04	0.8 – 1.4	Surficial	Apr, 2015	24	3
					Living	Apr, 2015	-	2
LMR	-	2.54	1.22	0.6 – 3.6	Surficial	May, 2014	18	5

Lady Musgrave Reef (LMR, Figure 1d) is a closed ring type with a single windward edge that has encircled to enclose and form a lagoon (Maxwell, 1968). Thus, the orientation of the platform and reef flats reflect the prevailing wind and swell direction. The reef contains an extensive, crescent shaped reef flat, which transitions directly into the sand apron (Table 1). The northern margin has a dredged channel (40 m wide, 9 m water depth), created in the early twentieth century (Steers, 1937). The reef platform (11 km^2) is composed of a lagoon (3 km^2) and substantial reef flats (Hamylton et al., 2016).

2.2. Field methods and sampling strategy

Sand apron samples in OTR were collected in approximately 50 m intervals from the algal flat to the lagoonward edge of the sand apron across three sand aprons (NSA, ESA, SSA), with 13 transects examined within this study (N = 83, Figure 2a, Table 1). Further, 'living' samples were collected from turfing algae of the reef flat and immediately desiccated in sunlight. Samples from LMR (N = 18) were collected from a point grid with 500 m spacing, in addition to several samples between points (Figure 2a, d, Table 1). No 'living' samples from the algal flat were obtained for LMR. For all surficial sediments, approximately 300 g of the upper 2.5 cm of sediment were collected and transported back to the University of Sydney and dried at 60°C for 48 hours. Samples were dry sieved for 0.5 - 2 mm, coinciding with the size range of LBF study species.

2.3. Taphonomic analysis

This study employed a categorical taphonomic index of test alteration (T_f), adapted from methods described in Fellowes et al. (2016). Family Calcarinidae (*B. sphaerulata, C. capricornia*[1] and *C. mayorii*) are the most abundant species in the Capricorn Bunker Group (Mamo, 2016) and account for up to 90% of LBFs within the sample. The loss of appendages and alteration of the test surface was analysed by allocating four categories of test condition (T_f = 1 – 4, 25 percentiles), with the assignment of taphonomic values provided in Table A1. Since morphological differences between two closely related *Calcarina* species (*Calcarina capricornia* and *mayorii*) are virtually indistinguishable with heavily abraded tests, they were recorded by genus. The index was applied to random samples of *B. sphaerulata* and *Calcarina spp.* for a total of 100 tests, with three replicates per sample. Several samples from the NSA and LMR contained less than 100 tests and the maximum possible number was observed, with those lower than 30 tests excluded from analyses. A

[1] Note that *C. capricornia* is a newly described species from the Capricorn Bunker Group, GBR bearing similarities and previously referred to as *Calcarina hispida* or *Calcarina splerengii* (Mamo, 2016).

197 weighted average (Eq. 1), biased towards more abraded tests, was used to determine the average
198 taphonomy across the sand apron:

199 $$T_f = \frac{(n_1)+(2n_2)+(3n_3)+(4n_4)}{N}$$ Equation 1

200 where, n_1 to n_4 are the sum of individuals belonging to each 'division' of abrasion (1 to 4) and N is
201 the total sample number. 'Living' specimens collected on the reef flat were pristine and assigned a
202 value of $T_f = 1$.

203 **2.4. Geochemical analyses**

204 **2.4.1. 'Living' LBF Sample preparation**

205 To ensure the sampling of 'living' foraminifera for geochemical analysis, individuals were hand-
206 picked for observable algal symbionts and pristine tests. The tests of living LBF (as opposed to sand
207 apron samples) are overlayed by an organic matrix, which is enriched in Mg^{2+}, removed using
208 methods modified from Raja et al. (2007). 'Living' LBF samples were initially rinsed in milli-Q
209 water three times and then treated in 1 ml buffered oxidizing agent (10% H_2O_2 and 0.1 M NaOH)
210 within a water bath (60□C) for 15 minutes. Subsequently, the tests were rinsed, then ultra-sonicated
211 in milli-Q water for 10 minutes. Great care was taken to ensure the spines and outer test wall
212 remained intact.

213 **2.4.2. Pooled test elemental ratios using ICP - AES**

214 A pool of 10 foraminifera, from either *B. sphaerulata* or *C. capricornia* were randomly picked from
215 each sample and crushed between two glass plates to homogenise the material. Approximately 1 mg
216 (± 0.2 mg) of the sample was digested in 10 ml of 2% NHO_3 for an hour before analysis. The
217 analysis was performed on a Varian Vista axially viewed plasma (AX) charged coupled device
218 (CCD) ICP–AES at the Australian National University, Canberra. Experimental runs were
219 performed on July 2015 and June 2016, with analytical conditions of 1.3kV power with Plasma Ar
220 flow of 15 L/min. Stabilization delay and uptake delay were 20 and 30 s respectively. Emission

lines of Ca (λ = 315.887 nm, 317.933 nm), Mg (λ = 285.213 nm) and Sr (λ = 407.771 nm, 421.552 nm) were used. Sample size for each analysis was 200 – 500 μL with an analysis time of 4 min per sample. There were 10 replicates per sample, with a delay time of 5 s. The relative element sensitivity for each element was calibrated with an in-house reference material ('Coral Std.',). Drift correction for each emission spectra was achieved through bracketing each measurement with Coral Std. and applying Eqn. A2. Mg/Ca and Sr/Ca quotient error was calculated according to Topping (1972). Minor element analyses within *B. sphaerulata* and *C. capricornia* tests for surficial samples are presented in Tables B1, B2.

2.4.3. Inter-test variability using EPMA, EDS and SEM

Tests from *B. sphaerulata* and *C. capricornia* were analysed for Mg, Sr and Ca on samples sourced from the algal flat and lagoonward edge of the SSA. Before analysis, test sections were embedded in epoxy resin on glass slides. Once the resin filled all chamber cavities, the specimens were polished using carborundum (silicon carbide) and aluminium oxide powder so that the internal, transverse chamber walls were exposed. Specimens were then carbon coated (50 nm) under vacuum evaporator. Compositional analyses (WDS for Mg, Ca and Sr), BSE imaging and WDS X-ray intensity maps of micro-bores were carried out using a JEOL JXA 8530F field emission electron microprobe in the Central Analytical Research Facility (CARF) at Queensland University of Technology, Brisbane (Australia) using Probe for EPMA software and ZAF matrix correction method (Armstrong/Love Scott). Analytical conditions were 10 kV accelerating voltage, 10 nA beam current, and a 10 μm defocused beam. Astimex mineral standards included dolomite (Mg Kα), calcite (Ca Kα) and celestite (Sr Kα). A coating thickness correction for 500 Å of carbon (ρ = 2.1) was specified for the unknowns in data reduction. Oxygen was calculated by cation stoichiometry and included in the matrix correction. Carbon was calculated 0.333 atoms relative to 1.0 atom of oxygen. Analytical totals using the carbon coat thickness correction average 99.5 wt.% ± 0.3 (1 s.d.; n = 49), and stoichiometric proportions calculated on the basis of three atoms of O per

formula unit yield an average atom sum of 4.996 ± 0.004. Average analytical sensitivities at the 99% confidence level for Sr, Ca and Mg were 470, 410 and 150 ppm respectively. Mapping conditions were 7 kV accelerating voltage, a beam current of 30 nA, a fully focused and fixed beam (stage mode) with a step size of 0.5 microns and a dwell time of 100 ms.

2.4.4. Statistical analysis and data visualisation

To determine relationships between Mg/Ca, Sr/Ca and the taphonomic index (T_f), linear regressions were employed. NSA, ESA and LMR were excluded from analysis due to low sample size and were only tested for Coefficient of determination (R^2). Mg/Ca and Sr/Ca were non-normally distributed ($p < 0.05$, Shapiro-Wilk test). However, linear regressions were still employed, as they remain robust against deviations from normality with an appropriate sample size (Underwood, 1997). Differences in Mg content in spines and test from EPMA data were determined using t-tests. Analyses were conducted using SPSS statistical package. 'Kernel Interpolation with barriers' within ArcMap v10.3 was used to interpolate and visualise taphonomy and elemental ratios across the sand aprons.

3. Results

3.1. Taphonomic analyses

Increasingly altered tests and thus increased average taphonomic values (T_f) were observed lagoonwards in all transects for both LBF groups analysed within the sand aprons of OTR and LMR (Figure 2), with the single exception of the genus *Calcarina* within the ESA (Figure 2c) at OTR. Lowest T_f (least altered) for each sand apron were found in samples closest to the algal flat and increased in value lagoonward, where highest values were observed at the lagoonward edge of each sand apron (Figure 2). The SSA exhibits a prominent NW gradient from algal flat to the lagoonward edge of the sand apron (Figure 2b, c). Similarly, the NSA and LMR exhibited lagoonward trends of

269 increasing T_f to the SW and NW respectively. The ESA exhibited a westerly gradient for *B.*
270 *sphaerulata*, whilst lacking any clear trend for *Calcarina spp.* (Figure 2b).
271
272 Variation in T_f values lagoonward differed markedly between sand aprons and LBF studied, where
273 the windward margins of OTR (SSA, ESA) generally presented larger ranges in T_f values relative to
274 the leeward margin (NSA) and LMR. Lightly abraded tests ($T_f = 2$) for both species were still
275 observed within samples approximately 60 and 100 m into the sand apron for ESA and SSA
276 respectively, whilst the NSA and LMR solely contained moderately to heavily altered tests ($T_f \geq 3$)
277 in all samples. The SSA contained the widest range, followed by the ESA, NSA, and LMR
278 respectively (Table 2). Thus, taphonomic gradients extend the entirety of the sand apron for both
279 the SSA and ESA, whilst they were restricted to less than 120 m from the reef flat within LMR and
280 NSA (Figure 2b, c). Lastly, *B. sphaerulata* and *Calcarina spp.* presented differences in the range of
281 T_f values within each sand apron, affecting the resolution of gradients lagoonward. Within OTR, *B.*
282 *sphaerulata* was generally less altered that *Calcarina spp.* (Table 2). Some transects, particularly
283 the ESA and NSA solely contained heavily abraded *Calcarina spp.* tests, where the lack in variation
284 leads to a lack in a clear T_f gradient lagoonward.
285

Figure 2. Interpolation of average taphonomic values (T_f) with sample sites outlined for One Tree Reef (**a**) and Lady Musgrave Reef (**d**). Interpolations for *Baculogypsina sphaerulata* (**b, e**) and *Calcarina spp.* (**c, f**) are shown for One Tree Reef and Lady Musgrave Reef. *Note that for T*f*, the genus Calcarina was composed of *C. capricornia* and *C. mayorii*.

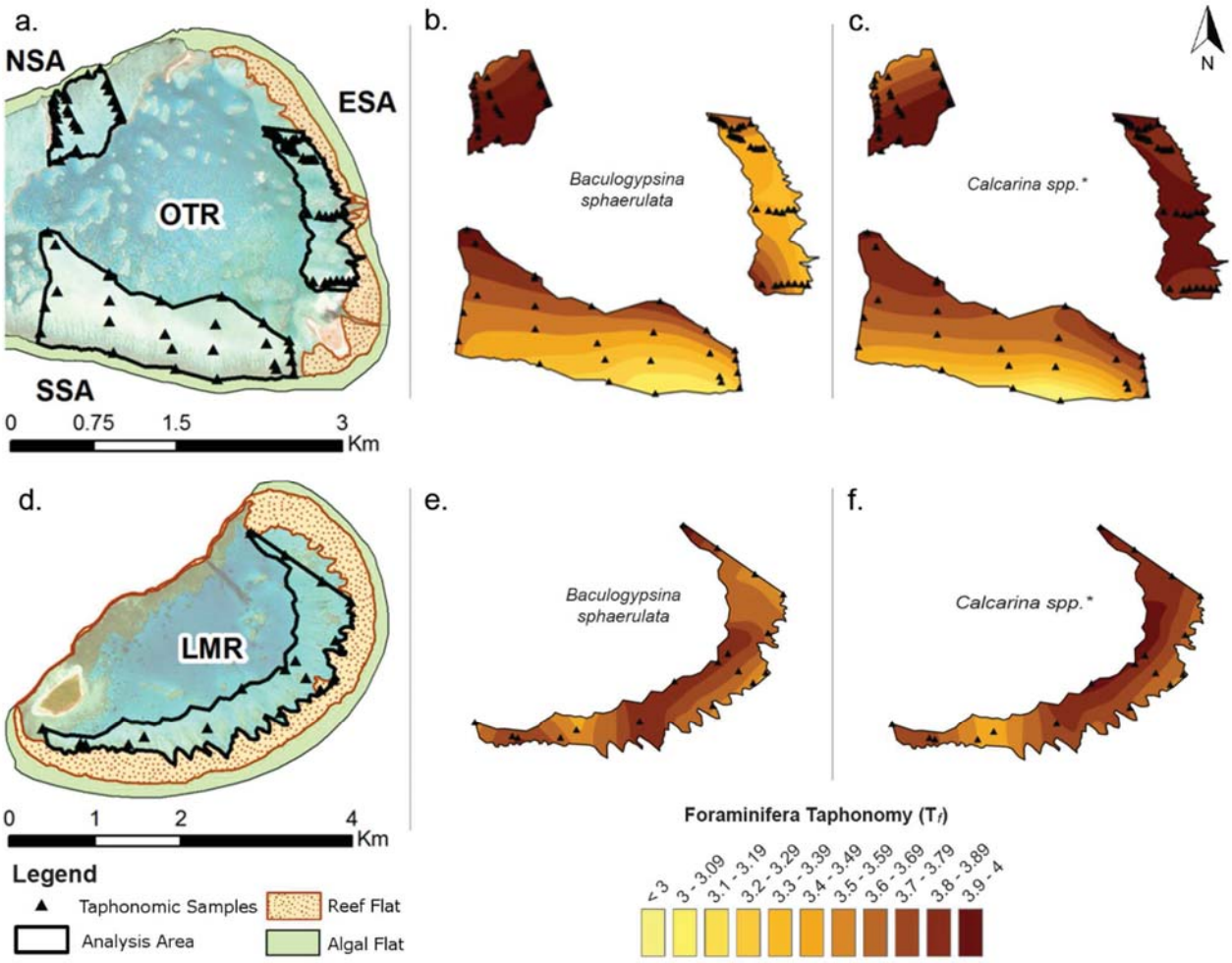

299 **3.2. Geochemical analyses**

300 Figure 3. Interpolation of Mg/Ca and Sr/Ca content within the tests of *Baculogypsina sphaerulata*
301 and *Calcarina capricornia*, detected using ICP-AES analyses. Sample sites are outlined for One
302 Tree Reef (**a**) and Lady Musgrave Reef (**b**). Mg/Ca interpolations (**c – f**) are presented for sand
303 aprons on One Tree Reef (**c, e**) and Lady Musgrave Reef (**d, f**) for both species. Sr/Ca
304 interpolations are also shown for One Tree Reef (**g, i**) and Lady Musgrave Reef (**h, j**) for both
305 species. Errors (RSD%) for each sample fall within the interval of the scale. Note that *C.*
306 *capricornia* was composed of *C. mayorii* during taphonomic analysis.

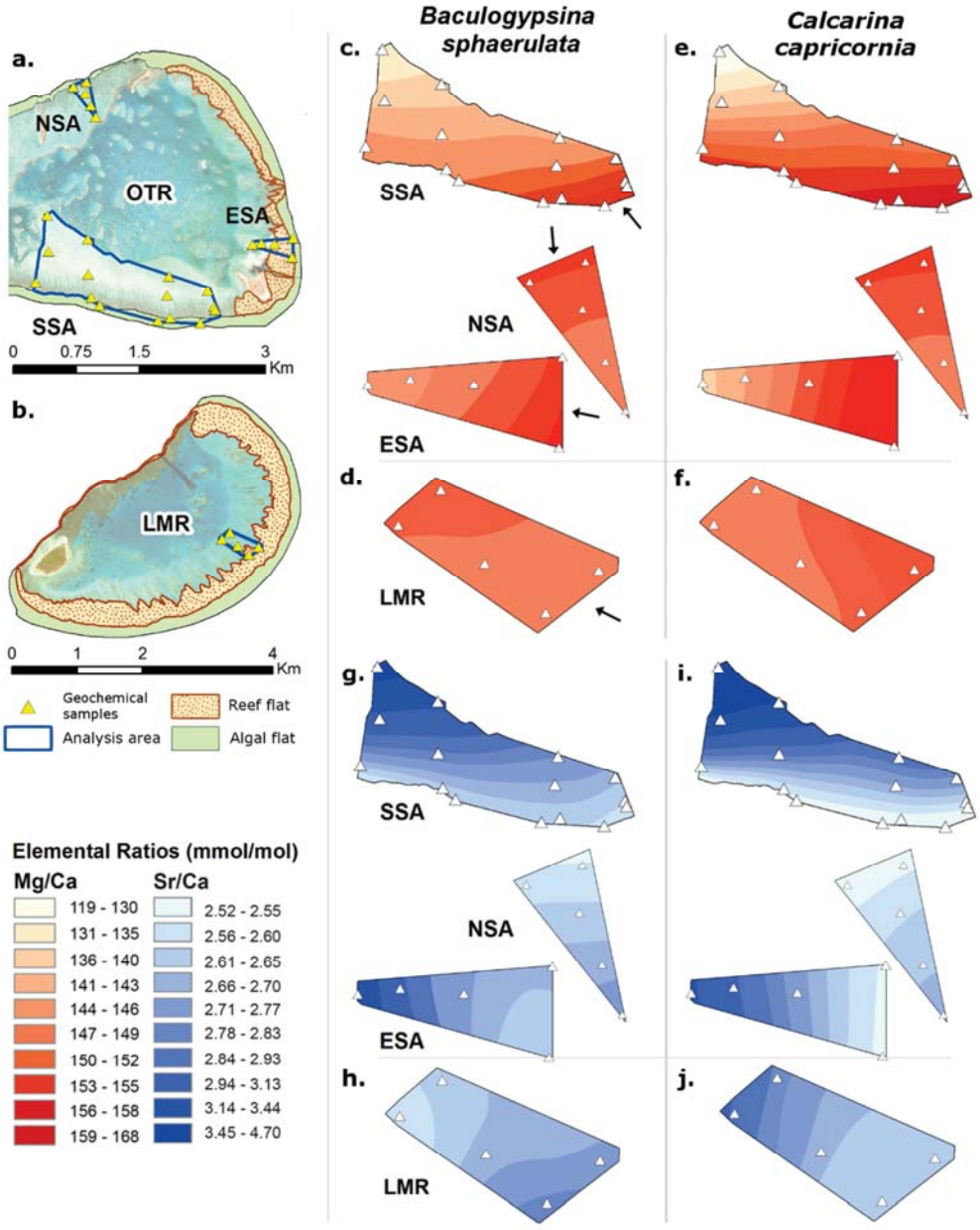

307

Table 2. Range of average taphonomy (T_f), Mg/Ca and Sr/Ca across all sand aprons and for both study species.

		Avg. Taphonomy (T_f)		Mg/Ca (mmol/mol)		Sr/Ca (mmol/mol)	
		Min	**Max**	**Min**	**Max**	**Min**	**Max**
Baculogypsina sphaerulata							
SSA	Living	-	-	148.87	164.37	2.60	2.69
	Surficial	3.09	3.94	134.97	164.37	2.60	3.70
ESA	Living	-	-	156.30	159.60	2.61	2.67
	Surficial	3.04	4.00	147.35	159.60	2.61	3.14
NSA	Living	-	-	155.61	156.73	2.54	2.58
	Surficial	3.51	4.00	148.70	156.73	2.54	2.74
LMR	Surficial	2.77	4.00	149.38	154.74	2.58	2.83
Calcarina capricornia							
SSA	Living	-	-	150.47	168.88	2.52	2.59
	Surficial	2.65	3.99	116.60	168.88	2.52	4.70
ESA	Living	-	-	163.28	165.33	2.53	2.53
	Surficial	3.59	4.00	140.88	165.34	2.53	3.29
NSA	Living	-	-	155.78	157.85	2.50	2.52
	Surficial	3.36	4.00	147.01	157.85	2.50	2.66
LMR	Surficial	3.16	3.98	149.96	156.68	2.55	2.95

3.2.1. Trends in Mg/Ca

Mg/Ca decreased lagoonward for all but one of the samples and was consistent between species. Highest ratios of Mg/Ca were found for live collected samples in the algal flat and lowest values on the lagoonward edge of sand aprons for tests of both species. The Mg/Ca of live collected (algal flat) samples for both species studied exhibited near identical ranges, although showed variability between the three algal flats of OTR. The southern algal flat exhibited greatest variability within 'living' tests at 156.47 ± 8.36 (s.d.) mmol/mol and 160.22 ± 8.92 (s.d.) mmol/mol for *B. sphaerulata* and *C. capricornia* respectively. In contrast, NSA and ESA algal flat samples deviated by 2.3 (s.d.) mmol/mol at most for both species (Table 2).

Within the sand apron, the Mg/Ca of the deposited tests decreased lagoonwards, in a NW direction for the SSA, whilst the ESA and NSA showed decreasing W and SW trends respectively (Figure 3c, e and f). Samples from LMR extended from within the reef flat (*c.f.* algal flat), to the edge of the sand apron and presented similar trends for *C. capricornia,* yet counter trends for *B. sphaerulata*

relative to those observed within OTR. Whilst *C. capricornia* decreased lagoonwards, *B. sphaerulata* saw a marginal increase, which counters all other transects within this study (Figure 3d). In terms of the range of values, the SSA exhibited the greatest variation across surficial sediments for both species, whilst the other three sand aprons analysed (ESA, NSA and LMR) were comparable in range for *B. sphaerulata* (Figure 3 c - f). However, inter-species variation was observed across all samples, where *C. capricornia* exhibits a larger decrease in Mg/Ca, relative to *B. sphaerulata*. The windward margins of OTR show larger decreases than both NSA and LMR (Table 2). Lastly, *C. capricornia* within the sand aprons contained a broad range of Mg/Ca values observed (116 - 168 mmol/mol), whilst for *B. sphaerulata* the range was lower (135 – 164 mmol/mol).

3.2.2. Trends in Sr/Ca

Increasing Sr/Ca in LBF tests is observed lagoonward, counter to each Mg/Ca counterpart (Figure 3g - i). The lowest Sr/Ca values are found for 'live collected' specimens from the algal flat, whilst highest values are observed for post-mortem tests on the lagoonward edge of the sand apron. However, the Sr/Ca ratios is two orders of magnitude lower than Mg/Ca, ranging from 2.50 – 4.70 mmol/mol and 2.55 – 3.95 mmol/mol for OTR and LMR respectively. Algal flat samples are less variable in Sr/Ca than Mg/Ca for both species, with Sr/Ca averaging 2.61 ± 0.05 (s.d.) and 2.53 ± 0.03 (s.d.) mmol/mol for *C. capricornia* and *B. sphaerulata* respectively across all sand aprons of OTR. Lagoonward trends of Sr/Ca align with Mg/Ca and taphonomy, with increasing values for the SSA in a NW direction, whilst the ESA and NSA show increasing W and SW trends respectively (Figure 3g, i). Whilst the elemental ratio gradients for both species are consistent within OTR, within LMR *B. sphaerulata* displays counter trends to *C. capricornia*. For the latter, Sr/Ca increases lagoonwards (2.55 to 2.95 mmol/mol), whilst *B. sphaerulata* tests decrease in Sr/Ca? marginally across the sand apron (2.83 to 2.56 mmol/mol).

The magnitude of change in Sr/Ca from reef and algal flat samples to those collected in the sand apron varies across sand aprons. A doubling in Sr/Ca is observed across the SSA for *C. capricornia*, with the highest value recorded at 4.70 mmol/mol, coinciding with the furthest sample from the algal flat. Whilst there is a marginal increase in Sr/Ca for the NSA and LMR, values are no greater than 3 mmol/mol for both species. Species differences are pronounced, as *C. capricornia* presents a wider Sr/Ca range (2.50 – 4.70 mmol/mol) than *B. sphaerulata* (2.54 – 3.70 mmol/mol) from algal flat to sand apron.

3.3. Relationships between Mg/Ca, Sr/Ca and Taphonomy

Significant correlations exist between the index of taphonomic alteration (T_f) and Mg/Ca and Sr/Ca for both species, although the relationship is non-linear in most sand aprons. There are significant, strong correlations between T_f and Mg/Ca for both species, whilst only *C. capricornia* displays weak yet significant relationships between T_f and Sr/Ca (Figure B1). Samples from LMR are only weakly correlated for both ratios, with the exception of Sr/Ca in *C. capricornia* ($R^2 = 0.703$).

3.4. EPMA, WDS and SEM: Spatial distribution of Mg and Sr content

SEM images of *B. sphaerulata* and *C. capricornia* show comparable test size and number of spines. EPMA analyses indicate elevated levels of Mg within spines of both species (Figure 4, Table 3), with significant differences for both *C. capricornia* ($t(9) = 6.83$, $p < 0.001$) and *B. sphaerulata* ($t(16.5) = 4.44$, $p < 0.001$). Epoxy-mounted transverse sections reveal naturally occurring pores (1- 2 µm) and larger internal chambers (25 - 40 µm), distributed systematically within both species (Figure 5a, c). Algal flat *B. sphaerulata* and *C. capricornia* tests exhibit no external and internal alteration (Figure 4) whilst 'altered' samples from the lagoonward edge of the sand apron contain extensive loss of spines and outer test wall (Figure 5, 6) and the presence of extensive microbial boring (Figure 6). Microbial bores (8 - 20 µm) are intermediate in size between the two naturally occurring pores and are most abundant at the test wall, decreasing in number towards the test centre (Figure 6b). Several bores display varied states of cement-infilling for both species, where SEM

images reveal the presence of acicular needles (1-2 µm in length, Figure 5d). WDS elemental maps further demonstrate elevated Sr and Ca, with reduced Mg within these cements (Figure 6).

Table 3. Electron microprobe spot analyses of tests and spines in *Baculogypsina sphaerulata* and *Calcarina capricornia* from the One Tree Reef. Tests were sourced from the algal flat, with unaltered appendages although treated. * number of spots analysed, [1] Oxygen calculated on the basis of cation stoichiometry, [2] Carbon calculated on the bases of 0.333 atoms C to 1 atom oxygen.

			Element wt. % (± 1 s.d.)					
Sample	**Species**	**n***	**Sr**	**Mg**	**Ca**	**O[1]**	**C[2]**	**TOTAL**
Tests								
3b	*B. sphaerulata*	3	0.21 (0.05)	3.05 (0.04)	35.1 (0.2)	48.7	12.3	99.3 (0.2)
3e	*C. capricornia*	3	0.20 (0.04)	3.00 (0.14)	35.1 (0.3)	48.7	12.3	99.2 (0.2)
3g	*B. sphaerulata*	3	0.21 (0.03)	3.08 (0.14)	34.9 (0.1)	48.7	12.3	99.2 (0.1)
3h	*B. sphaerulata*	3	0.21 (0.02)	3.07 (0.02)	35.2 (0.2)	48.7	12.2	99.4 (0.2)
3j	*C. capricornia*	5	0.23 (0.03)	3.02 (0.07)	35.1 (0.3)	48.7	12.3	99.3 (0.2)
Spines								
3b	*B. sphaerulata*	9	0.17 (0.04)	3.08 (0.06)	35.5 (0.4)	48.8	12.2	99.7 (0.4)
3e	*C. capricornia*	5	0.20 (0.04)	3.22 (0.06)	35.4 (0.2)	48.8	12.2	99.9 (0.2)
3g	*B. sphaerulata*	5	0.17 (0.02)	3.23 (0.04)	35.0 (0.4)	48.8	12.3	99.5 (0.4)
3h	*B. sphaerulata*	4	0.19 (0.04)	3.16 (0.10)	34.9 (0.1)	48.7	12.3	99.3 (0.1)
3j	*C. capricornia*	4	0.18 (0.03)	3.21 (0.04)	35.0 (0.2)	48.8	12.3	99.5 (0.1)

Figure 4. Mg vs. Ca (wt. %) in foraminiferal tests (blue) and spines (red) from the algal flat (pristine), as measured by electron microprobe (samples detailed in Table 6). Error bars are ±1 s.d.

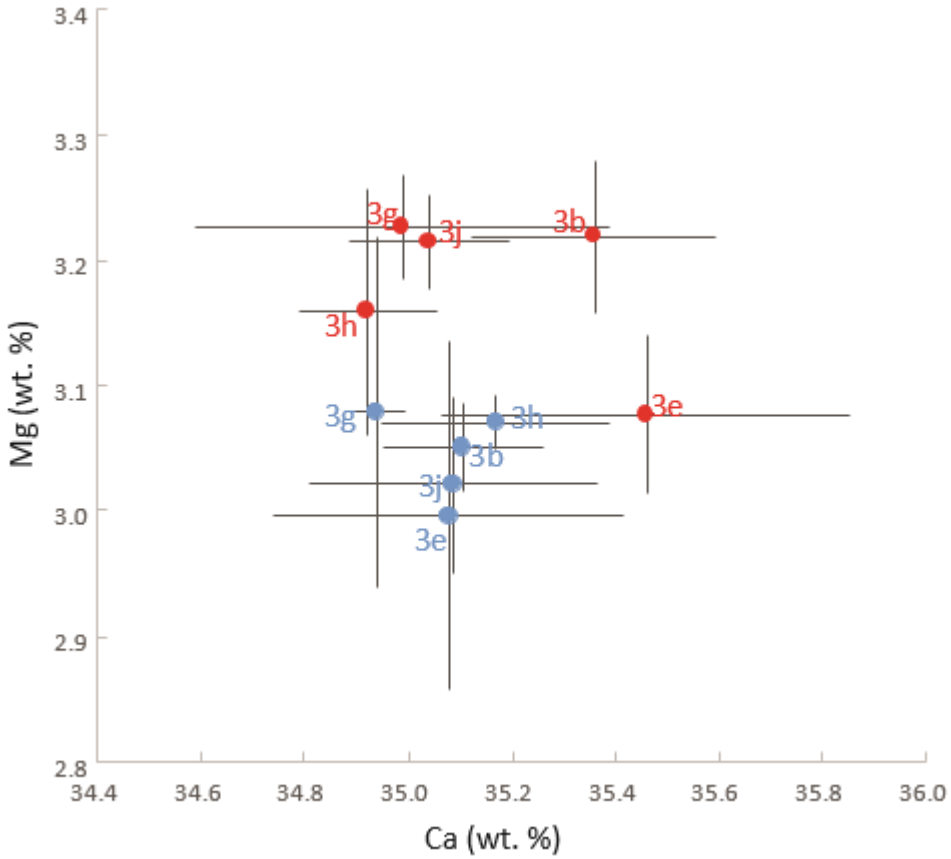

Figure 5. Back-scattered electron (BSE) image of the transverse sections of *Calcarina capricornia* and *Baculogypsina sphaerulata* tests. Comparisons of unaltered algal flat samples for *C. capricornia* (**a**) and *B. sphaerulata* (**c**), with an altered sand apron sample (**b**), showing internal microbial boring (1) and loss of spines and outer test wall (2*)*. Acicular, needle cements in *C. capricornia* (**d**)*,* showing partially infilled (3) and completely infilled bores (4). Red markers in (**a**) and (**c**) indicate spot locations for EPMA analysis within the spines and test.

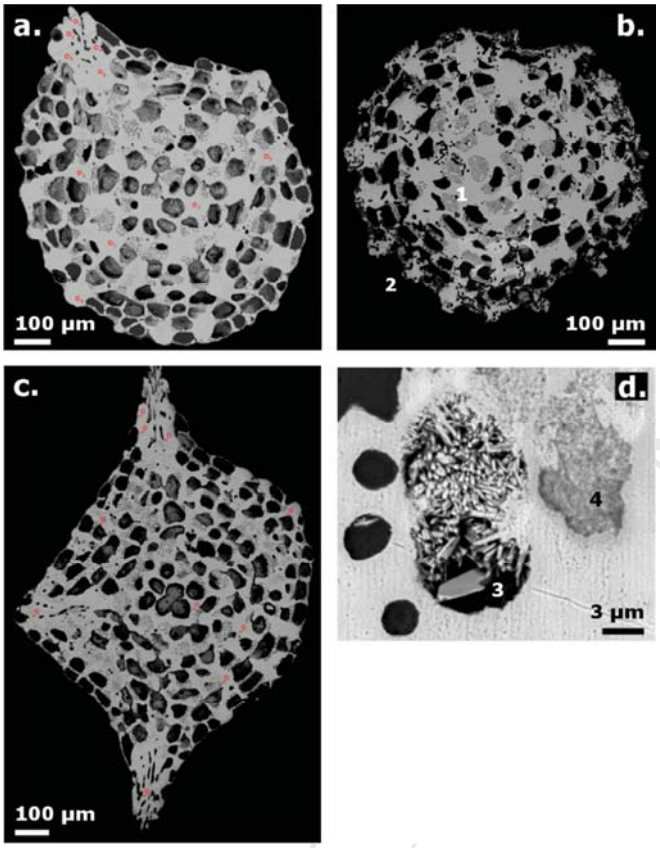

Figure 6. Back-scattered electron (BSE) images (a, b) and corresponding Wavelength-dispersive X-ray spectroscopy (WDS) elemental maps of Ca (c, d), Sr (e, f) and Mg (g, h) of infilled microbial bores in *Baculogypsina sphaerulata* (**a, c, e, g**) and *Calcarina capricornia* (**b, d, f, h**). BSE images (**a**) show partially and completely infilled bores (*arrows*). Elemental maps of the same areas show elevated Ca and Sr and lower Mg within the infilled bores relative to tests. Colour scale bars at right indicate relative intensities. Scale bars are 100 µm.

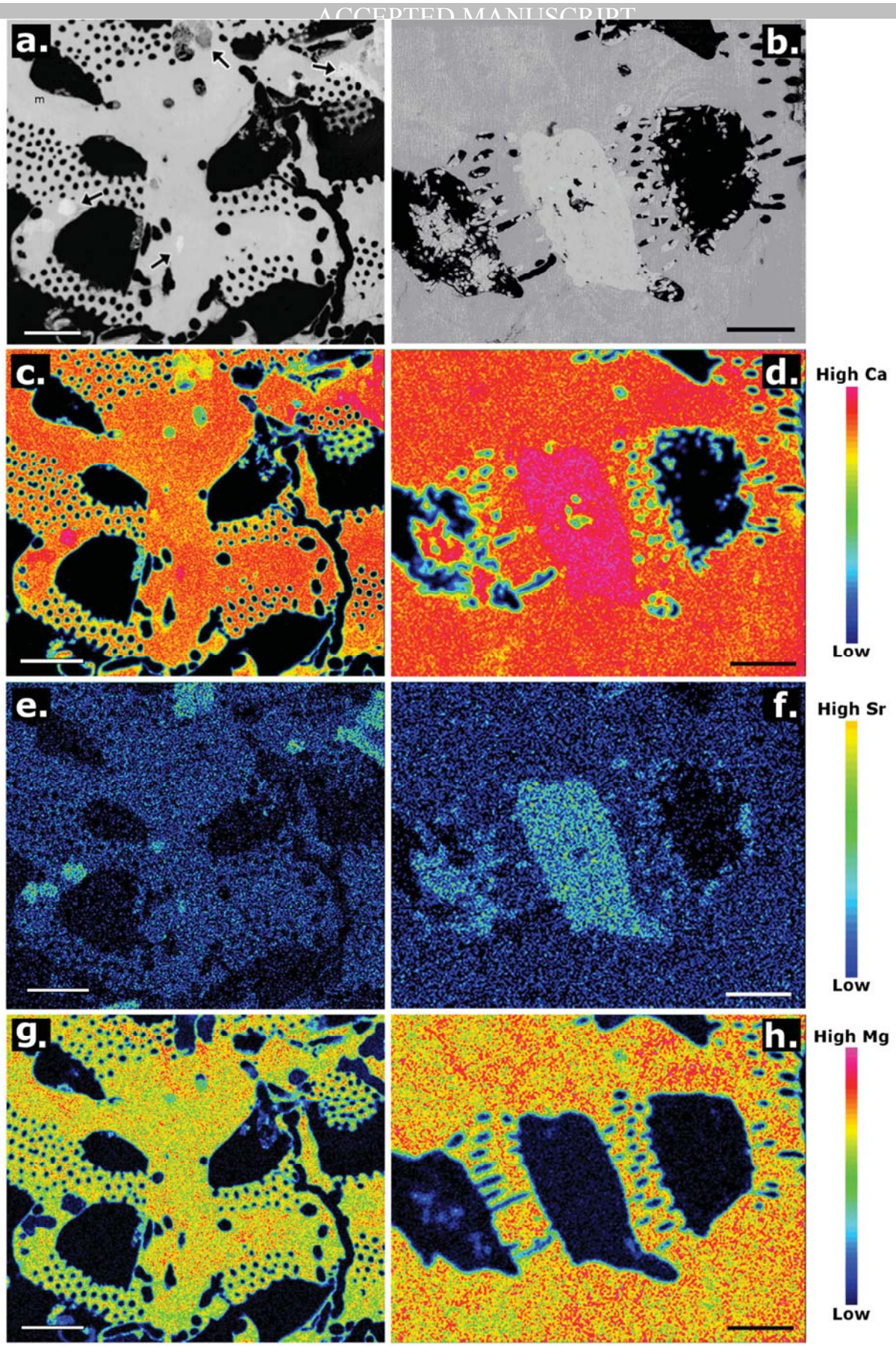

405

4. Discussion

4.1. Inferring Transport Pathways

4.1.1. Taphonomic Analyses

Within One Tree and Lady Musgrave reefs, the tests of *B. sphaerulata* and *Calcarina spp.* show increasing alteration in test condition lagoonwards across each sand apron. These trends vary in direction, length and magnitude of change, which reflect the variability of the prevailing wave climate on each sand apron. For example, the windward SSA is the most extensively prograded sand apron (Vila-Concejo et al., 2013), producing a clear NW taphonomic gradient from algal flat (T_f = 2.8 – 3.1) to sand apron (T_f = 4) for both species. As a windward margin, the SSA receives the most wave forcing throughout the year, whilst the NW gradient aligns with previously described wave refraction across the reef flat and into the sand apron (Harris et al., 2015). Similarly, the southern area of the ESA exhibits a westerly gradient lagoonward, driven by the easterly swell component within the region. These findings are consistent with other studies on One Tree Reef , elsewhere on the GBR (Pilarczyk et al., 2014, Dawson et al., 2014), Caribbean (Li et al., 1998) and Okinawa (Fujita et al., 2009), reaffirming the suitability of taphonomic gradients to infer potential sediment transport pathways within carbonate environments.

Figure 7. Conceptual model of the taphonomic alteration of a LBF test from algal flat (source) to back-reef sand apron (sink). Wave forcing transports LBF tests into the back-reef, exposing the test to mechanical abrasion and microbial boring, which may cause a decrease in Mg/Ca and Sr/Ca test content. An existing proxy to infer transport pathways is a qualitative index of taphonomic abrasion (T_f = 1 – 4). However, we propose that the changes in Mg/Ca and Sr/Ca ratios may be an advantageous proxy to infer sediment transport within the back-reef environment. Taphonomic values described in Table A1, with *Baculogypsina sphaerulata* images adapted from Fellowes *et al.* (2016).

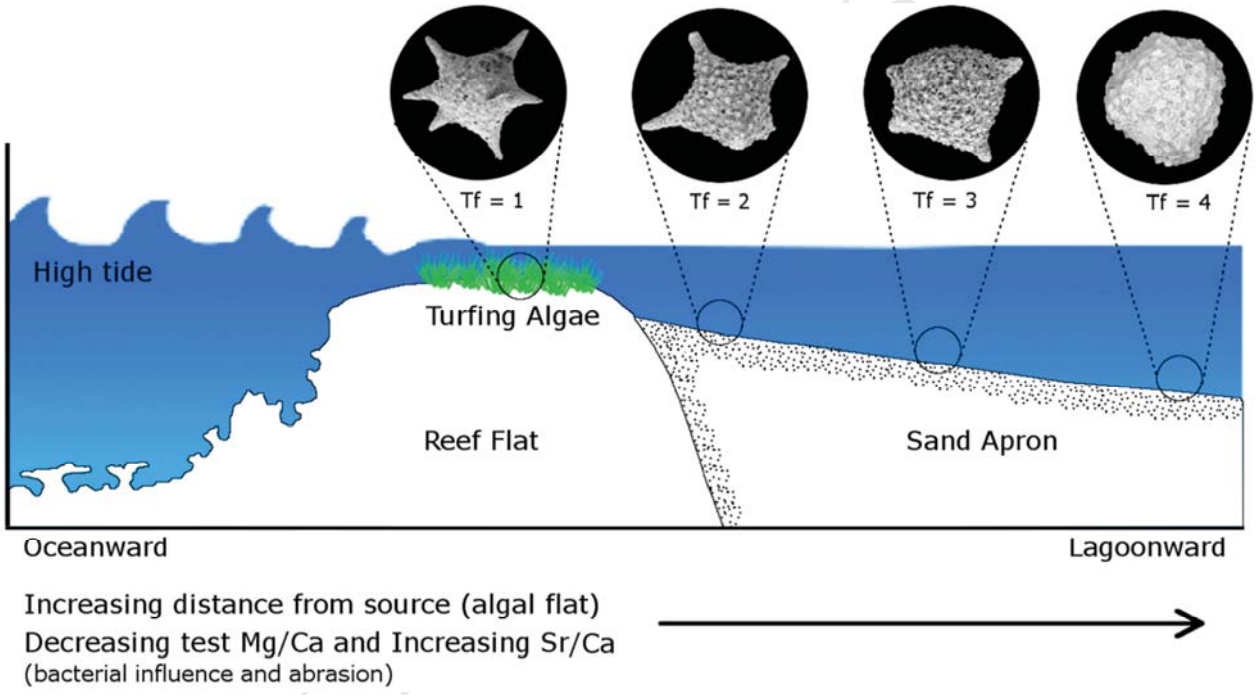

However, the use of T_f in discerning pathways across the entire sand apron is limited by test contribution from the algal flat and a lack of variation in T_f values. For example, the entire extent of the NSA and LMR contained highly abraded tests ($T_f \geq 3$), limiting the inference of pathways to 100 m from the reef flat (Figure 2b, c). Further, the ESA, *Calcarina spp.* displays marginally decreasing T_f lagoonwards (T_f= 3.9 to 3.7, *i.e.* increasingly pristine tests), which is counter to their source area and direction of wave forcing. Both these trends can be explained by the low contribution of LBF into the sand apron, where Fellowes et al. (2016) indicates reduced *Calcarina spp*. within the ESA and NSA, which Doo et al. (2016) report as reduced populations within the corresponding algal flats. Therefore, a low abundance of LBF, combined with a narrow range of taphonomic values (*i.e.* all heavily abraded) prevents the inference of transport pathways, which we suggest may be addressed through geochemical means.

4.1.2. ICP-AES: Mg/Ca and Sr/Ca as indicators of sediment transport

Whilst observing increasing taphonomic alteration across the back-reef sand apron, this study simultaneously demonstrates decreasing Mg/Ca and increasing Sr/Ca across almost all sand aprons. Pristine, unaltered tests on the algal flat contain the highest and lowest values of Mg/Ca and Sr/Ca respectively, whilst highly altered tests at the lagoonward edge of each sand apron show the inverse for these ratios (Figure 3). In discerning the direction of potential transport pathways and magnitude of wave forcing, both Mg/Ca and Sr/Ca effectively match taphonomic gradients lagoonward. Within OTR, the SSA showed a clear NW gradient, the southern portion of the ESA exhibited a westerly gradient, whilst the NSA showed a southerly gradient for both Mg/Ca and Sr/Ca. All three gradients coincide with known prevailing wave climate and wave refraction (Harris et al., 2014). These trends extend further to neighbouring LMR, where *C. capricornia* also demonstrates a clear NW gradient lagoonward.

As with taphonomy, the magnitude of change for both elemental ratios varies across each sand apron, which suggests these ratios are indicative of wave forcing intensity. Again, the SSA presents

468 the largest decrease and increase of Mg/Ca and Sr/Ca respectively, from algal flat to sand apron
469 (Table 2), with both ratios significantly correlating with taphonomy lagoonwards (Table B3, Figure
470 B1). The observed doubling of Sr/Ca across the sand apron and large loss of Mg/Ca may be driven
471 in part by the length of the sand apron and thus transport distance. In contrast, the NSA contains a
472 far narrower range of values (Figure 2b, c), which may result from low wave-energy modal
473 conditions. Similarly, LMR has the narrowest range of values, with minimal change in the
474 lagoonward gradient of *C. capricornia* and insignificant relationships between both ratios and
475 taphonomy (Figure 3, Table B3). Thus, a narrower range in values and weaker correlation with
476 taphonomy may be indicative of lower wave forcing intensity and transport distance, with similar
477 trends in the two reefs.
478
479 There are several key differences between elemental ratios and T_f, where the former allow the
480 observation of gradients despite low LBF contribution. As explored earlier, *Calcarina spp.* within
481 the ESA demonstrates a counter-trend to *B. sphaerulata* with more pristine tests lagoonwards,
482 driven by low test abundance (Fellowes et al., 2016). Nevertheless, analysis of Mg/Ca and Sr/Ca
483 within *C. capricornia* shows clear westerly gradients lagoonwards (Figure 3), mirroring sediment
484 pathways inferred from the more abundant *B. sphaerulata* species (Figure 2b). Similarly, the
485 leeward NSA contained low abundance and a narrow range in T_f values, limiting the inference of
486 transport pathways. However, in using both elemental ratios in both reefs, potential pathways are
487 identified across the entirety of the sand apron. The greatly reduced need for test material (ten tests
488 per sample vs. > 30 for taphonomy) overcomes limitations in low LBF contribution within the sand
489 apron.
490
491 Since T_f is a discrete, categorical measure, the index lacks the ability to fully capture the spectrum
492 of heavily abraded tests, leading to a lack of variation across the entirety of the sand apron and thus
493 restricts the inference of transport pathways. In contrast, Mg/Ca and Sr/Ca capture the full extent of

494 test alteration across the sand apron. For example, the greatest amount of change was observed
495 within the SSA, with a decrease of up to 50 mmol/mol in Mg/Ca and doubling of values for Sr/Ca
496 (Table 2). In comparison, the ESA and NSA contains successively lower ranges in Mg/Ca,
497 coinciding with intermediate and low wave forcing (Table 2). Thus, elemental analyses are
498 independent of abundance and allow for the full extent of analysis of test alteration.
499
500 In analysing LMR, two contrasting transects were found; *C. capricornia* mirrored trends within
501 OTR whilst *B. sphaerulata* displayed opposite trends: namely increasing Mg/Ca and decreasing
502 Sr/Ca from the same samples across the sand apron (Figure 3). The magnitude of change for both
503 ratios was relatively small (Table 2), although *B. sphaerulata* showed a particularly weak
504 relationship between Mg/Ca (R^2 = 0.045) and Sr/Ca (R^2 = 0.284) with taphonomy. Possible
505 explanations are differences in *B. sphaerulata* source areas or the influence of a large man-made
506 channel on the leeward margin of LMR. A recent digital elevation model (DEM) by Hamylton et al.
507 (2016) reveals that the LMR samples reside at a lower depth of 0.3 – 0.6 m BSL, relative to the
508 surround area, leading to reduced wave exposure. Doo et al. (2016) suggest that *B. sphaerulata* are
509 abundant in algal flats of higher wave energy, relative to *C. capricornia*, which may lead to the
510 source areas of *B. sphaerulata* adjacent to the sampled transect. Another possible influence is the
511 presence of the large man-made channel along the leeward margin of LMR. The U-shaped channel
512 (12 x 34 m, depth x width) imposes strong influences on lagoonal currents during ebbing and
513 flooding tides. From the DEM of Hamylton et al. (2016), the conservative average ebbing/flooding
514 current velocity over the channel would be 1.6 m/s (using a lagoonal volume of $3x10^6$ m^2 and
515 spring tidal range of 3 m). Thus, there is a potential for considerably larger maximum velocities
516 over the tidal cycle, leading to the 'reverse' trends observed. The considerable influence they exert
517 over lagoonal transport is observed with sediment sorting, that was indicative of alongshore, rather
518 than across-shore transport where the transects were sampled (Hamylton et al., 2016). Thus, these

519 current pattern encourage cross-shore rather than onshore transport for *B. sphaerulata* whilst, *C.*
520 transport remains lagoonwards due to ample supply from the algal flat.
521

522 **4.2. Mechanisms for elemental ratio variation**

523 **4.2.1. EPMA: Mg/Ca trends through transport and dissolution**

524 Alteration of the test surface and loss of spines on all sand apron tests are indicative of transport
525 across the rough reef flat, due to mechanical abrasion. Experiments using shaker tables with LBF
526 tests (Peebles and Lewis, 1991) and carbonate sand (Kotler et al., 1992, Ford and Kench, 2012) as
527 the substrate mix links mechanical abrasion to the extensive loss in appendages, test weight and
528 smoothing of the test surface. Thus the loss of spines through physical transport may be the primary
529 driver for decreasing Mg/Ca in the tests across the sand apron. However, Kotler et al. (1992)
530 suggests that mechanical abrasion alone cannot account for significant taphonomic alteration. Since
531 transport distance from algal flat to sand apron is relatively short, chemical dissolution will also
532 drive losses in Mg content.
533

534 Using EPMA, *in situ* measurements of Mg content between LBF tests and spines indicates an
535 increase of 2.9% and 6.8% for *B. sphaerulata* and *C. capricornia* respectively (Figure 5 & 6, Table
536 3). Whilst alive, LBF test show considerable buffering capacity against test dissolution (Engel et al.,
537 2015). However, the LBF species investigated contain calcite with high levels of Mg (Mg-calcite),
538 which is the most unstable carbonate phase and most susceptible to dissolution (Zhang and Dawe,
539 2000). Tynan and Opdyke (2011) established that Mg-calcite dissolution initiated at pH values
540 lower than 8.2 pH, with Morse et al. (2006) hypothesising sequential dissolution, initiating with the
541 highest Mg content until the least soluble phases remain. As Mg-calcite, the tests of *B. sphaerulata*
542 and *C. capricornia* are an extremely vulnerable constituent of back-reef sediments and thus
543 potentially selectively dissolved with the diurnal fluctuation of lagoonal seawater pH (Price et al.,

544 2012). Further, Mg concentrations on specific microstructures may lead to the selective dissolution
545 of appendages, weakening test integrity which may further enhancing susceptibility to physical
546 abrasion (Kotler et al., 1992), resulting in the rough surface textures and pitted test walls observed
547 within this study.

548 **4.2.2. Sr/Ca – Microbial diagenesis**

549 Extensive microboring is present within sand apron LBF samples, with several bores indicating
550 different states of cement infilling (Figure 5, 6). The acicular, needle-like cements and elevated Sr
551 within all infillings suggest the cements are aragonitic, which mineralises with Sr content similar to
552 ambient sea water and thus far greater Sr content than Mg-calcite (Perry, 2000). Within carbonate
553 platforms, physical breakdown predominates along the high-energy windward reef flat, whilst
554 biological breakdown through micro-boring dominates lagoonal settings (Perry, 2000). Post-
555 mortem, LBFs are rapidly subjected to microbial decay, as the organic materials lining the internal
556 chambers and outer membrane are decomposed by algal, sponge and bacterial species (Reid and
557 MacIntyre, 1998). Colonization of such bore holes in carbonate environments creates a network of
558 small cavities which may allow for the development of cements (Nothdurft et al., 2007, Nothdurft
559 and Webb, 2009, McCutcheon et al., 2016). Previous analyses of micro-bored *Archaias angulatus*
560 (Family Sortidae) from the Bahamas bank showed significant post-depositional increases of up to
561 42% in aragonite content and a subsequent tenfold increase in Sr content from living to deposited
562 foraminifera (Reid and MacIntyre, 1998). Thus, through endolithic boring and subsequent aragonite
563 cementation, LBF grains may significantly increase in Sr content across a sand apron.

564 **4.2.3. Species-specific Differences**

565 Whilst both study species presented near identical trends in elemental composition lagoonwards, the
566 magnitude of change was greater in *C. capricornia*. Both species are closely related (Family
567 Calcarinidae), with identical mineralogy (Mg-calcite) and near identical values for both Mg/Ca and
568 Sr/Ca within 'living' samples on the algal flat. However, *C. capricornia* contains more

microstructures on the test surface (Figure 4a, 5b), which increases the surface available for chemical reactivity. Further, *C. capricornia* contains a layer of canals which connect the inner chambers with the ambient seawater, which is absent in *B. sphaerulata* (Röttger and Krüger, 1990). Lastly, *B. sphaerulata* possesses smaller internal chamber space relative to *C. capricornia* (Figure 4), which limits the surface area available for reaction and cementation. These characteristics may explain the larger variability in elemental ratios observed in *C. capricornia*. Other inter-species considerations include organic coatings and shapes of individual crystallites within pore spaces, which have significant effects on dissolution resilience (Henrich and Wefer, 1986).

4.3. Future directions

The elemental ratios as a proxy for sediment transport have the potential to be used across different reef regions, with several applications. As seen in this study, the ratios provide evidence for the direction of wave forcing, intensity and influences on transport patterns from source to sink. An extension of these proxies is the analysis of LBF tests down-core, which together with taphonomic analysis may reveal the depositional dynamics and allow novel measures of sedimentation rates and sub-surface grain alteration. These results also indicate the effects of early diagenesis in LBF tests, which may be used to understand sub-surface diagenesis, with implications on the use of LBFs for dating. An understanding of LBF dynamics and their contribution to the sediment dynamics provides insights towards the geomorphological evolution of the reef, in addition to sediment dynamic responses to altered environmental conditions. However, the inherent variability within LBF must be taken into account before comparing different reefs. Raja et al. (2007) reports Mg/Ca values for *B. sphaerulata* at over 250 mmol/mol and demonstrates seasonal variation ranging up to 40 mmol/mol, from the same site. These values are far greater than those found within this study and may be driven by phylogeny and local conditions. Thus, future applications must first establish a baseline for each species with a thorough analysis of the elemental composition of living LBF specimens at each study site.

5. Conclusion

This study shows that Mg/Ca and Sr/Ca within LBF tests are valid proxies for inferring both the direction and local dynamics of sediment transport and holds several advantages over previously employed measures, such as a taphonomic index. Decreasing Mg/Ca and increasing Sr/Ca was observed lagoonwards, across two neighbouring, yet distinct reefs within the Capricorn Bunker Group, Great Barrier Reef. Furthermore, both ratios possess a significant relationship with taphonomy, suggesting they may complement or even replace taphonomy as a proxy. EPMA analyses indicate elevated Mg content in spines relative to tests, which contribute to physical and chemical alteration through preferential dissolution. Further, WDS mapping and SEM imaging reveal increased Sr content in aragonite cement infilling of microbial bores. Comparison of the use of elemental ratios versus taphonomy illustrates that the former method requires minimal test material and provides a continuous measure, capturing a greater extent of test alteration, and reveals pathways that are otherwise undetected by the taphonomic index. These proxies may be applied to different reef regions and the extension of their use downcore may provide novel insights to sediment dynamics on coral reefs, contributing to a greater understanding of their morphological evolution.

6. Acknowledgements

Vila-Concejo's ARC Future Fellowship (FT100100215) and Women in Science programme, in addition to Webster's ARC Grant (DP1094001) and Start up fund from the University of Sydney funded this work. EPMA data reported in this paper were obtained at the Central Analytical Research Facility (CARF) operated by the Institute for Future Environments (QUT). Access to CARF is supported by funding from the Science and Engineering Faculty (QUT). LMR samples acquired using Hamylton's Return to Work Grant, from the University of Wollongong. Special thanks to Steve Doo, Adriana Dutkiewicz, Kate Paz, Roberta Johnson, Naomi Huynh and Amanda

Thran for the insightful discussions and comments. Thanks to the assistance of SAB volunteers in the field. Fieldwork was undertaken at One Tree Island Research Station, a facility of The University of Sydney.

7. References

ALEJO, I., AUSTIN, W. E. N., FRANCÉS, G. & VILLAS, F. 1999. Preliminary Investigations of the Recent Foraminifera of Baiona Bay, N.W. Spain. *Journal of Coastal Research,* 15**,** 413-427.

BRIGUGLIO, A. & HOHENEGGER, J. 2011. How to react to shallow water hydrodynamics: the larger benthic foraminifera solution. *Marine Micropaleontology,* 81**,** 63-76.

CHUN, L., JONES, B. & BLANCHON, P. 1997. Lagoon-shelf sediment exchange by storms; evidence from foraminiferal assemblages, east coast of Grand Cayman, British West Indies. *Journal of Sedimentary Research,* 67**,** 17-25.

DAWSON, J. L., SMITHERS, S. G. & HUA, Q. 2014. The importance of large benthic foraminifera to reef island sediment budget and dynamics at Raine Island, northern Great Barrier Reef. *Geomorphology,* 222**,** 68-81.

DOLAN, E. & CHARLES, H. F. 2003. Longshore Sediment Transport Rates on a Reef-Fronted Beach: Field Data and Empirical Models Kaanapali Beach, Hawaii. *Journal of Coastal Research,* 19**,** 649-663.

DOO, S. S., HAMYLTON, S. & BYRNE, M. 2012. Reef-scale assessment of intertidal large benthic foraminifera populations on One Tree Island, Great Barrier Reef and their future carbonate production potential in a warming ocean. *Zoological Studies,* 51**,** 1298-1307.

DOO, S. S., HAMYLTON, S., FINFER, J. & BYRNE, M. 2016. Spatial and temporal variation in reef-scale carbonate storage of large benthic foraminifera: a case study on One Tree Reef. *Coral Reefs***,** 1-11.

ENGEL, B. E., HALLOCK, P., PRICE, R. E. & PICHLER, T. 2015. Shell dissolution in larger benthic foraminifers exposed to ph and temperature extremes: Results from an in situ experiment. *The Journal of Foraminiferal Research,* 45**,** 190-203.

EREZ, J. 2003. The source of ions for biomineralization in foraminifera and their implications for paleoceanographic proxies. *Reviews in mineralogy and geochemistry,* 54**,** 115-149.

FELLOWES, T. E., GACUTAN, J., HARRIS, D. L., VILA-CONCEJO, A., WEBSTER, J. M. & BYRNE, M. 2016. Patterns of Sediment Transport Using Foraminifera Tracers across Sand Aprons on the Great Barrier Reef. *Journal of Coastal Research,* 0**,** null.

FORD, M. R. & KENCH, P. S. 2012. The durability of bioclastic sediments and implications for coral reef deposit formation. *Sedimentology,* 59**,** 830-842.

FUJITA, K., OSAWA, Y., KAYANNE, H., IDE, Y. & YAMANO, H. 2009. Distribution and sediment production of large benthic foraminifers on reef flats of the Majuro Atoll, Marshall Islands. *Coral Reefs,* 28**,** 29-45.

HAMYLTON, S. M., CARVALHO, R. C., DUCE, S., ROELFSEMA, C. M. & VILA‐CONCEJO, A. 2016. Linking pattern to process in reef sediment dynamics at Lady Musgrave Island, southern Great Barrier Reef. *Sedimentology,* 63**,** 1634-1650.

HARRIS, D., VILA-CONCEJO, A., WEBSTER, J. & POWER, H. 2015. Spatial variations in wave transformation and sediment entrainment on a coral reef sand apron. *Marine Geology,* 363**,** 220-229.

HARRIS, D., WEBSTER, J., DE CARLI, E. & VILA-CONCEJO, A. 2011. Geomorphology and morphodynamics of a sand apron, One Tree reef, southern Great Barrier Reef. *Journal of Coastal Research***,** 760 - 764.

HARRIS, D. L., VILA-CONCEJO, A. & WEBSTER, J. M. 2014. Geomorphology and sediment transport on a submerged back-reef sand apron: One Tree Reef, Great Barrier Reef. *Geomorphology,* 222**,** 132-142.

HENRICH, R. & WEFER, G. 1986. Dissolution of biogenic carbonates: effects of skeletal structure. *Marine Geology,* 71**,** 341-362.

HOPLEY, D. 1982. *The geomorphology of the Great Barrier Reef: Quaternary development of coral reefs*, John Wiley & Sons.

HOPLEY, D., SMITHERS, S. G. & PARNELL, K. 2007. *The geomorphology of the Great Barrier Reef: development, diversity and change*, Cambridge University Press.

KENCH, P. S. & BRANDER, R. W. 2006. Wave processes on coral reef flats: implications for reef geomorphology using Australian case studies. *Journal of Coastal Research,* 22**,** 209-223.

KOTLER, E., MARTIN, R. E. & LIDDELL, W. D. 1992. Experimental analysis of abrasion and dissolution resistance of modern reef-dwelling foraminifera: implications for the preservation of biogenic carbonate. *Palaios***,** 244-276.

LI, C., JONES, B. & KALBFLEISCH, W. B. C. 1998. Carbonate sediment transport pathways based on foraminifera: Case study from Frank Sound, Grand Cayman, British West Indies. *Sedimentology,* 45**,** 109-120.

LUDINGTON, C. 1979. Tidal Modifications and Associated Circulation in a Platform Reef Lagoon. *Marine and Freshwater Research,* 30**,** 425-430.

MAIKLEM, W. 1968. Some hydraulic properties of bioclastic carbonate grains. *Sedimentology,* 10**,** 101-109.

MAMO, B. L. 2016. Benthic Foraminifera from the Capricorn Group, Great Barrier Reef, Australia. *2016,* 4215**,** 123.

MARSHALL, J. & DAVIES, P. 1982. Internal structure and Holocene evolution of One Tree Reef, southern Great Barrier Reef. *Coral Reefs,* 1**,** 21-28.

MAXWELL, W. G. H. 1968. *Atlas of the Great Barrier Reef,* London, Graham Henderson publishers.

MCCUTCHEON, J., NOTHDURFT, L. D., WEBB, G. E., PATERSON, D. & SOUTHAM, G. 2016. Beachrock formation via microbial dissolution and re-precipitation of carbonate minerals. *Marine Geology,* 382**,** 122-135.

MORSE, J. W., ANDERSSON, A. J. & MACKENZIE, F. T. 2006. Initial responses of carbonate-rich shelf sediments to rising atmospheric pCO 2 and "ocean acidification": Role of high Mg-calcites. *Geochimica et Cosmochimica Acta,* 70**,** 5814-5830.

NOTHDURFT, L. D. & WEBB, G. E. 2009. Earliest diagenesis in scleractinian coral skeletons: implications for palaeoclimate-sensitive geochemical archives. *Facies,* 55**,** 161-201.

NOTHDURFT, L. D., WEBB, G. E., BOSTROM, T. & RINTOUL, L. 2007. Calcite-filled borings in the most recently deposited skeleton in live-collected Porites (Scleractinia): Implications for trace element archives. *Geochimica et Cosmochimica Acta,* 71**,** 5423-5438.

ORME, G., FLOOD, P. & EWART, A. 1974. An investigation of the sediments and physiography of Lady Musgrave Reef: a preliminary account. *Proc. 2nd Int. Coral Reef Symp.*

PEEBLES, M. W. & LEWIS, R. D. 1991. Surface textures of benthic foraminifera from San Salvador, Bahamas. *The Journal of Foraminiferal Research,* 21**,** 285-292.

PERRY, C. T. 2000. Factors Controlling Sediment Preservation on a North Jamaican Fringing Reef: A Process-Based Approach to Microfacies Analysis. *Journal of Sedimentary Research,* 70**,** 633-648.

PERRY, C. T., SPENCER, T. & KENCH, P. 2008. Carbonate budgets and reef production states: a geomorphic perspective on the ecological phase-shift concept. *Coral Reefs,* 27**,** 853-866.

PILARCZYK, J. E., GOFF, J., MOUNTJOY, J., LAMARCHE, G., PELLETIER, B. & HORTON, B. P. 2014. Sediment transport trends from a tropical Pacific lagoon as indicated by Homotrema rubra taphonomy: Wallis Island, Polynesia. *Marine Micropaleontology,* 109**,** 21-29.

PRICE, N. N., MARTZ, T. R., BRAINARD, R. E. & SMITH, J. E. 2012. Diel Variability in Seawater pH Relates to Calcification and Benthic Community Structure on Coral Reefs. *PLOS ONE,* 7**,** e43843.

RAJA, R., SARASWATI, P. K. & IWAO, K. 2007. A field‐based study on variation in Mg/Ca and Sr/Ca in larger benthic foraminifera. *Geochemistry, Geophysics, Geosystems,* 8.

RAJA, R., SARASWATI, P. K., ROGERS, K. & IWAO, K. 2005. Magnesium and strontium compositions of recent symbiont-bearing benthic foraminifera. *Marine Micropaleontology,* 58**,** 31-44.

RANKEY, E. C. & GARZA-PÉREZ, J. R. 2012. Seascape metrics of shelf-margin reefs and reef sand aprons of Holocene carbonate platforms. *Journal of Sedimentary Research,* 82**,** 57-75.

REID, R. P. & MACINTYRE, I. G. 1998. Carbonate recrystallization in shallow marine environments: A widespread diagenetic process forming micritized grains. *Journal of Sedimentary Research,* 68**,** 928-946.

RÖTTGER, R. & KRÜGER, R. 1990. Observations on the biology of Calcarinidae (Foraminiferida). *Marine Biology,* 106**,** 419-425.

STEERS, J. A. 1937. The Coral Islands and Associated Features of the Great Barrier Reefs. *The Geographical Journal,* 89**,** 1-28.

STORLAZZI, C. D., OGSTON, A. S., BOTHNER, M. H., FIELD, M. E. & PRESTO, M. 2004. Wave-and tidally-driven flow and sediment flux across a fringing coral reef: Southern Molokai, Hawaii. *Continental Shelf Research,* 24**,** 1397-1419.

TOPPING, J. 1972. *Errors of observation and their treatment,* London, Chapman and Hall.

TYNAN, S. & OPDYKE, B. N. 2011. Effects of lower surface ocean pH upon the stability of shallow water carbonate sediments. *Science of the Total Environment,* 409**,** 1082-1086.

UNDERWOOD, A. J. 1997. *Experiments in ecology: their logical design and interpretation using analysis of variance*, Cambridge University Press.

VILA-CONCEJO, A., HARRIS, D. L. & POWER, H. E. Sand transport in coral reefs: Are lagoons infilling? Symposium on Coastal Sediment Processes, 2015 San Diego, California, USA.

VILA-CONCEJO, A., HARRIS, D. L., POWER, H. E., SHANNON, A. M. & WEBSTER, J. M. 2014. Sediment transport and mixing depth on a coral reef sand apron. *Geomorphology,* 222**,** 143-150.

VILA-CONCEJO, A., HARRIS, D. L., SHANNON, A. M., WEBSTER, J. M. & POWER, H. E. 2013. Coral reef sediment dynamics: evidence of sand-apron evolution on a daily and decadal scale. *In:* CONLEY, D. C., MASSELINK, G., RUSSELL, P. E. & O'HARE, T. J. (eds.) *Proceedings 12th International Coastal Symposium.* Plymouth, England: Journal of Coastal Research,.

VILA‐CONCEJO, A. & KENCH, P. 2017. Storms in Coral Reefs. *Coastal Storms: Processes and Impacts***,** 127-149.

ZHANG, Y. & DAWE, R. A. 2000. Influence of Mg 2+ on the kinetics of calcite precipitation and calcite crystal morphology. *Chemical Geology,* 163**,** 129-138.

APPENDIX A: METHODS

Table A1. Qualitative criterion for each division within the Taphonomic index for test alteration (Tf). These measures apply to spined LBF morphologies such as *B. sphaerulata* and *C. capricornia*. Adapted from Fellowes *et. al* (2016).

Index (T_f)	Qualitative criterion
1 (Pristine)	• Unaltered test surface, observable symbionts • All radial spines are present and unaltered
2 (Lightly abraded)	• Minimal alteration to test surface • Alteration and loss of radial spines (< 50%) • Absent or minimal pitting to test surface
3 (Moderately abraded)	• Moderate alteration to test surface • Evidence of pitting and fractures on outer test wall • Majority of radial spines (> 50%) lost • Any remaining spines are severely altered
4 (Heavily abraded)	• Significant alteration to test surface • No radial spines remain • Partial or complete removal of outer test wall

ICP-AES Quality control: Sample drift correction

To correct for sample drift, an initial fifty measurements of Coral Std, with additional measurements bracketing each sample. Drift was subsequently corrected (??$_{??????}$) to the known value of the standard, assuming drift throughout the run was linear using Eq. A1.

$$R_{cor} = \frac{R_{int}}{(S_{avg}/S_{known})} \qquad \text{Equation. A1}$$

where, R_{int} is the initial ratio of the sample, S_{avg} is the average of the ratios of the bracketing Coral Std. before and after the sample and S_{known} is the known ratio of the standard. Analytical precision was attained through a comparison of relative standard deviations (% RSD) with Coral Std. (n = 65, for both experimental runs) where all values fell within 2σ of known values.

Table B.1. Mg/Ca and Sr/Ca of a pool (n = 10) of *Baculogypsina sphaerulata* and *Calcarina hispida* tests from One Tree Reef, determined by ICP - AES

Sample name	Sr/Ca (mmol/mol)	RSD% (mmol/mol)	Mg/Ca (mmol/mol)	RSD% (mmol/mol)
Southern Sand Apron, OTR				
Baculogypsina sphaerulata				
SL1	2.6010	0.0914	164.3658	0.0265
SL5	2.6211	0.0010	148.8704	0.0838
SL9	2.6941	0.0140	149.6413	0.0782
2.2	2.5984	0.0443	151.3927	0.0020
2.4	2.6293	0.0070	153.1873	0.0108
2.5	2.6093	0.0612	150.8415	0.0294
4.3	2.8953	0.0558	142.7022	0.1397
4.5	2.6075	0.0210	149.5895	0.0188
4.7	2.6233	0.0006	153.3559	0.0300
8.2	3.0459	0.0190	143.9235	0.0110
8.4	2.6455	0.0578	147.2675	0.0246
8.6	2.6859	0.0322	144.5072	0.0446
10.1	3.6993	0.0715	134.9697	0.0030
10.4	3.0126	0.0763	141.7078	0.1564
10.8	2.6177	0.0820	148.6333	0.0783
Calcarina hispida				
SL1	2.5229	0.0713	168.8813	0.0814
SL5	2.5537	0.1309	150.4702	0.1220
SL9	2.5874	0.1338	154.9321	0.1830
2.2	2.8262	0.0366	152.5772	0.0174
2.4	2.5419	0.0319	151.9246	0.0397
2.5	2.5269	0.0890	150.7521	0.0314
4.3	3.0227	0.0258	146.9796	0.0530
4.5	2.5741	0.0078	151.7139	0.0127
4.7	2.5195	0.0351	155.9843	0.0114
8.2	3.0346	0.0345	140.9594	0.0071
8.4	2.5912	0.0146	153.1901	0.0147
8.6	2.5728	0.0503	150.2368	0.0423
10.1	4.7015	0.0843	116.6037	0.1207
10.4	3.1049	0.0843	144.6149	0.2078
10.8	2.6168	0.0208	149.9112	0.0306
Eastern Sand Apron, OTR				
Baculogypsina sphaerulata				
EL1	2.6700	0.0373	156.2991	0.0070
EL2	2.6105	0.0086	159.5985	0.0058
4.2	2.6342	0.0677	147.4799	0.0016
4.5	2.6837	0.0161	149.5707	0.0192
4.7	3.1355	0.0599	147.3476	0.0719
Calcarina hispida				
L1	2.5328	0.0057	163.2807	0.0407
L2	2.5336	0.0336	165.3357	0.0124
4.2	2.6930	0.0309	152.4469	0.0042
4.5	2.7706	0.1436	146.7125	0.0918
4.7	3.2909	0.0081	140.8813	0.0331
Northern Sand Apron, OTR				
Baculogypsina sphaerulata				
NL1	2.5759	0.0612	155.6056	0.0008
NL2	2.5385	0.0551	156.7333	0.0181
3.1	2.6366	0.0834	148.6961	0.2094
3.2	2.6667	0.1269	149.2337	0.2159
3.3	2.7444	0.1593	152.6881	0.0482
Calcarina hispida				
NL1	2.5020	0.1032	155.7804	0.2293
NL2	2.5190	0.1435	157.8455	0.2415
3.1	2.6443	0.0325	147.0146	0.0119
3.2	2.6635	0.1112	153.4785	0.1330
3.3	2.6513	0.0294	149.5407	0.1742

Table B2. Mg/Ca and Sr/Ca of a pool (n = 10) of *Baculogypsina sphaerulata* and Calcarina *hispida* tests from Lady Musgrave Reef, determined by ICP - AES

Sample name	Sr/Ca (mmol/mol)	RSD% (mmol/mol)	Mg/Ca (mmol/mol)	RSD% (mmol/mol)
Lady Musgrave Reef				
Baculogypsina sphaerulata				
L7B	2.6310	0.1130	154.7443	0.0105
L13B	2.6210	0.1067	150.5050	0.0158
L1B	2.5619	0.1496	151.9261	0.1169
L2B	2.8295	0.0165	149.6184	0.0657
L3B	2.6999	0.0728	149.3783	0.0489
Calcarina hispida				
L7C	2.7931	0.0252	151.5521	0.1644
L13C	2.5669	0.0882	151.3707	0.0280
L1C	2.9513	0.0132	149.9595	0.0542
L2C	2.6028	0.0695	152.8293	0.0564
L3C	2.5523	0.0579	156.8613	0.1126

Table B3. Results of linear regressions between average taphonomy (T_f) against Mg/Ca and Sr/Ca for surficial samples. ESA, NSA and LMG were only analysed for Coefficient of determination (R^2) due to low sample size. *Number of pooled samples analysed.

		Mg/Ca		**Sr/Ca**	
	n*	**p value**	**R^2**	**p value**	**R^2**
B. sphaerulata					
All	31	**< 0.0001**	0.386	0.065	0.104
OTR	26	**< 0.0001**	0.443	0.052	0.115
SSA	16	**0.006**	0.383	0.138	0.890
ESA	5	-	0.885	-	0.229
NSA	5	-	0.748	-	0.645
LMG	5	-	0.045	-	0.284
C. capricornia					
All	31	**0.001**	0.365	**0.019**	0.107
OTR	26	**0.001**	0.389	**0.023**	0.158
SSA	16	**0.016**	0.304	0.140	0.149
ESA	5	-	0.765	-	0.431
NSA	5	-	0.667	-	0.979
LMG	5	-	0.179	-	0.703

Figure B1. Relationships between Mg/Ca and Sr/Ca with an index for taphonomic alteration (Tf), with regression and coefficient of determination values presented in Table B3. Relationships are shown for the SSA (A, B), ESA (C, D), NSA (E, F) and LMG (G, H) for Mg/Ca and Sr/Ca respectively.

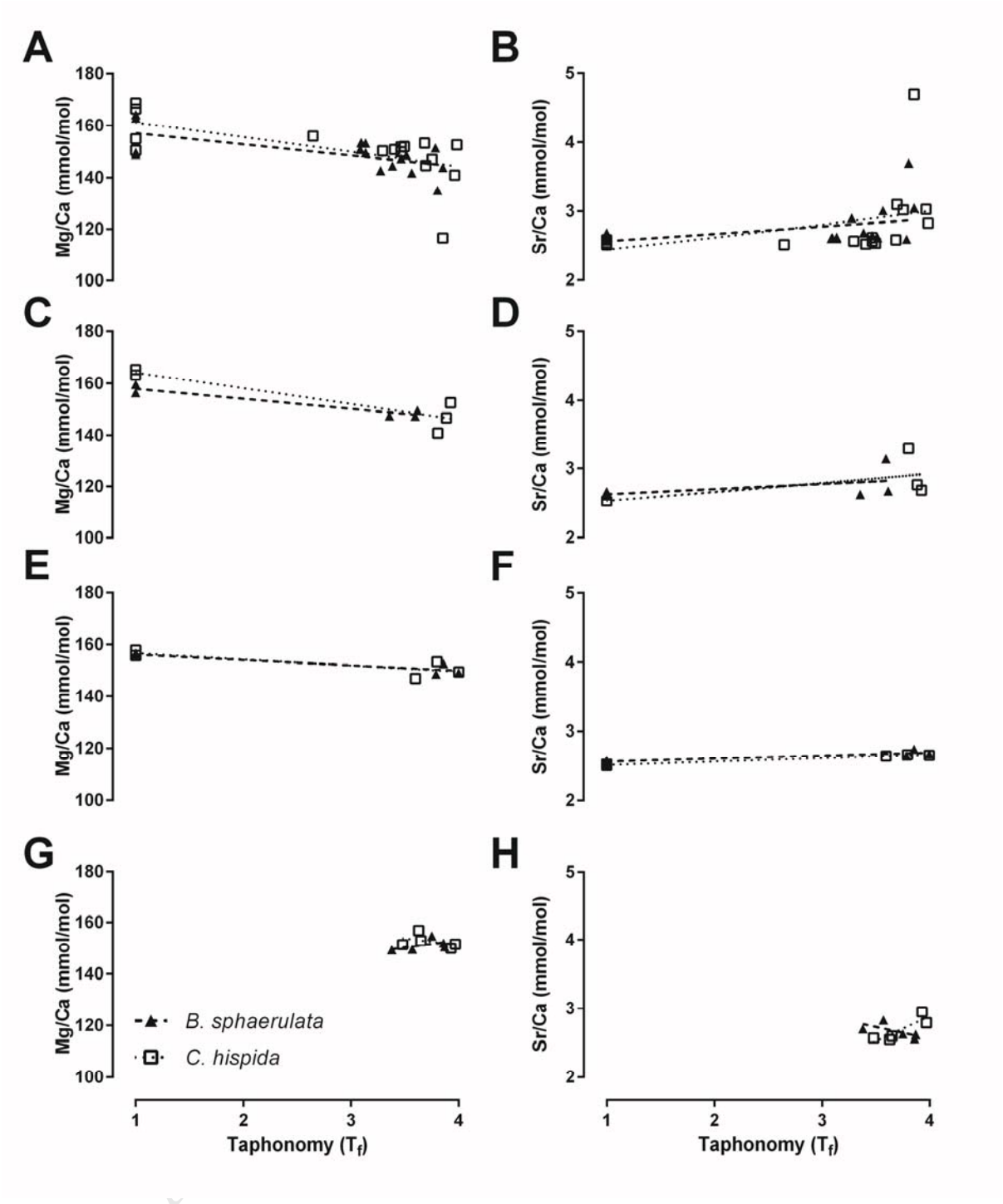

Highlights:

Using Mg/Ca and Sr/Ca of large benthic foraminifera to successfully infer sediment transport pathways.

The novel proxies overcome several limitations of traditional proxies

Physical and chemical forces may drive Mg/Ca trends, whilst differences in Sr/Ca driven by aragonite cementation